MAKING FULLERENE ION ENGINES WORK

M. W. Crofton and B.B. Brady
Technology Operations, Mechanics & Materials Technology Center
The Aerospace Corporation, P.O. Box 92957
Los Angeles, California 90009

Abstract

Means to achieve improved thrust density and enhanced efficiency are discussed for ion engines utilizing extraction grids. High mass propellants offer well-known potential benefits, but all previous attempts to utilize heavy molecules have failed to produce a laboratory device with performance approaching the current xenon standard. The chemistry of C_{60} fullerene molecules in the discharge chamber is analyzed, including the reactions of ionization, electron attachment, electron and ion recombination, and charge transfer. The CHEMKIN modeling program for chemical kinetics is used as an aid for the evaluation of engine feasibility. The analysis suggests that a positive fullerene ion engine can be constructed with performance figures much better than has been obtained in past attempts. Intense C_{60}^- sources can be constructed by similar means, although beam neutralization requires a large emission area and high energy expenditure which may limit its usefulness for spacecraft propulsion.

Nomenclature

A_m	main extraction area of ion engine, cm^2
A_n	neutralizer emission area, cm^2
B	magnetic field, gauss
d	discharge chamber diameter, cm
e	elementary charge, Coulomb or esu
E_0	initial total energy, J
g	acceleration of standard gravity, ms^{-2}
$\overline{g}$	mean relative velocity of collision partners, cms^{-1}
I_{sp}	specific impulse, s
k	boltzmann constant, JK^{-1}
k_a	rate coefficient for electron attachment, cm^3s^{-1}
k_i	rate coefficient for electron impact ionization, cm^3s^{-1}
k_r	rate coefficient for electron-ion recombination, cm^3s^{-1}
$k_{+/-}$	rate coefficient for ion-ion recombination, cm^3s^{-1}
l	distance between ion production and extraction sites, cm
m_i	mass of ionized propellant molecule or atom, kg
m_e	electron mass, kg
n_{60}	number density of C_{60}, cm^{-3}
N_e	total electron number density, cm^{-3}
N_i	total ion number density, cm^{-3}
N_m	total number density of Maxwellian electrons, cm^{-3}
N_p	total number density of primary electrons, cm^{-3}
N_{60}	C_{60} number density, cm^{-3}
N_{Xe^+}	number density of Xe+, cm^{-3}
N_{Xe}	number density of Xe, cm^{-3}
n_{60}^+	number density of C_{60}^+, cm^{-3}
n_{60}^-	number density of C_{60}^-, cm^{-3}
$n_e(\varepsilon)$	Maxwellian electron number density as a function of energy, cm^{-3}
r_c	electron cyclotron radius, cm
R	grid span to gap ratio
R_c	critical distance of closest approach for collision partners
s	length of drift region
S	C_{60} sublimation rate, $cm^{-2}s^{-1}$
T_a	thrust per unit extraction area, mN/cm^2
T_i	ion temperature, K
t_d	elapsed time between ion creation and extraction
V_N	neutralizer extraction voltage
V_{60}	C_{60} extraction voltage
v	velocity, cm/s
v_b	Bohm velocity, cm/s
z_i	elementary charge multiple for the ith ion
$d\varepsilon$	infinitesimal interval of electron energy, $(\varepsilon + d\varepsilon) - \varepsilon$, electron volts
ε	electron kinetic energy, electron volts
ε_m	maxwellian electron temperature (kT_e/e), electron volts
ε_p	primary electron energy (kT_e/e), electron volts
ε_0	permittivity constant, $C^2N^{-1}m^{-2}$
η_{tp}	thrust to power ratio, mN/kW
μ	reduced mass for collision pair, kg

Introduction

In a typical ion engine, xenon gas is ionized by electron impact in a plasma region. The xenon ions are extracted and accelerated with a series of charged grids downstream of the plasma region. These engines are capable of about 55% thrust efficiency at $I_{sp} \approx 3000$ s, with η_{tp} and T_a (thrust to power ratio and thrust per unit extraction area) of about 40 mN/kW and 0.3 mN/cm^2, respectively.[1-3] Efficiency at the optimal specific impulse for orbit transfer (1500-2000 s) is much lower.

Ideal propellant for these ion engines has a large ionization cross section and low ionization potential, low cross section for electron attachment, low recombination cross section for the singly charged ion, little fragmentation in an electrical discharge, high molecular mass, space storability, and convenient means of supply to the engine. Atomic rather than molecular propellants have been used almost exclusively, with insignificant attachment, recombination, and fragmentation rates. Xenon is widely recognized as the best propellant presently available for practical ion thrusters. Nevertheless, large performance improvements are possible for a high-mass molecular propellant with suitable properties when utilized in a properly designed engine.

Background

The favorable features for ion propulsion using the molecular propellant C_{60}, a recently discovered carbon allotrope, have been described previously.[1] Based on a 720.7 amu molecular mass and 7.6 eV ionization energy, the potential efficiency is much higher than for xenon, particularly at $I_{sp} \leq 3000$ s. However, intensive research and development efforts directed at fullerene ion propulsion have at best produced engines which operate at low efficiency levels and have serious propellant deposition and other problems.[4-6] All C_{60} engines have had low T_a levels due to an inability to produce and extract C_{60}^+ at high current densities. Fragmentation occurs due to the ~1 ms residence time of C_{60} and the likely occurrence of multiple collisions with electrons during this period.[4,6] RF ion engines built to reduce fragmentation effects by avoiding the use of high temperature hollow cathodes have also been inefficient.[4,5] Due to the large C_{60} electron attachment cross section, RF discharges in a xenon/C_{60} mixture were strongly quenched. The wall as well as propellant feed line of these engines has been heated to maintain the desired C_{60} vapor pressure for suitable operation without excessive deposition. At the required temperature, typically 800-1000 K, thermal radiation losses cause a significant drain on engine efficiency. Fragmentation and deposition rates inside the thruster have been high enough to more than nullify the efficiency gain expected with this propellant, and could lead to early thruster failure.

The potential benefits of using higher propellant mass in ion engines, increased thrust density and efficiency, are well known. Using Child's law, ion engine thrust can be expressed as a function of specific impulse, I_{sp}, grid span-to-gap ratio, R, and propellant unit mass, m_i:

$$T = \frac{\pi \varepsilon_0}{18}(R)^2\left(\frac{m_i}{e}\right)^2(gI_{sp})^4 \qquad (1)$$

R, the ratio of extraction grid diameter to the grid spacing, is normally the factor limiting achievable thrust density for xenon ion engines. Currently, practical grid systems do not use R greater than several hundred, because of potential grid shorting problems caused by thermal distortion. Propellants are usually compared by holding the specific impulse fixed, since this is a fundamental mission parameter. An ion engine operating on C_{60} then has the potential to provide 30 times higher thrust density than an engine operating on xenon (same R in each case). In a mixed propellant engine, the thrust contributions from the two ion types are additive although the I_{sp} will not be the same for each propellant. If the utilization and ion beam current are the same for each species, xenon I_{sp} will be higher than C_{60} I_{sp} in a xenon-C_{60} engine by $\sqrt{5}$, and the average I_{sp} will be 1.7 times that of C_{60}. At the same average I_{sp}, the mixed propellant engine still provides a space charge limited thrust considerably higher than the pure xenon engine, with roughly equal contributions coming from each species. Due to the high C_{60} mass, thrust can be increased by raising I_{sp} at a substantially lower cost in added power input. With a 50-50 mix and the same beam current, utilization, and I_{sp}, the engine would provide 2.3 times the thrust level of a pure xenon engine. For a pure C_{60} engine, it is 5.5 times higher. The power input to maintain specific impulse level, neglecting any increase in energy cost per extracted ion, is only 17% greater, so that thrust to power ratio is increased by a factor of 2.0.

The propellant loss and residue formation observed in fullerene engines built to-date results primarily from the electron impact ionization process that has been used in all cases. To achieve acceptable ionization efficiency, the C_{60} is bombarded by energetic electrons in a plasma. The electron energy distribution function inside a typical ion engine

discharge chamber is double-peaked, with one maximum around 30 eV, and another at about 5 eV.[7] C_{60} is unusually stable with respect to fragmentation, requiring 45 eV of internal energy to undergo ionization and subsequent fragmentation by C_2 ejection.[8] The electron impact ionization of C_{60} by a single 30 eV electron at modest thermal temperatures (≤ 1000 K) will produce little fragmentation on a microsecond time scale but the fragmentation yield may be substantial on the millisecond timeframe[6,8] (also, thermal degradation of C_{60} deposits eventually occurs at continuous temperatures on the order of 1000 K and above.[9]) In the designs employed to-date for a C_{60} ion engine, the residence time is on the order of a millisecond. The problem of C_{60}^+ fragmentation in the thruster would clearly be reduced if the ions were extracted more rapidly after their creation, preferably with a residence time of ≤10 microseconds.

Analysis of the Production and Extraction of Fullerene Ions

In the conventional gridded ion engine, propellant ions predominantly in the +1 charge state are produced by electron impact ionization. Significant ionization occurs in the entire primary electron region, which is the discharge chamber portion enclosed by the grid system and magnetic field lines that intersect the anode.[10] Low energy electrons have higher probability of crossing magnetic field lines, and are gradually released to wall surfaces and the low-field drift region near the grids. These ions migrate toward the screen grid at roughly the Bohm velocity during extracted beam operation. With atomic propellants, negligible electron-ion recombination occurs in the low field region. An orificed hollow cathode discharge usually serves as the primary source of ionizing electrons, with additional electrons supplied from propellant ionization in the main discharge region.

Electron Impact Ionization

The electron impact ionization cross section for C_{60}^+ formation

$$C_{60} + e \rightarrow C_{60}^+ + 2e \qquad (2)$$

is large, 5.5×10^{-15} cm^2 at 38 eV,[11,12] with an appearance energy of 7.61 eV. The corresponding cross section for Xe is an order of magnitude lower.[13]

The C_{60}^+/C_{60} ionization rate coefficient can be obtained from

$$k_i = \langle \sigma_i v_e \rangle = \frac{\int_0^\infty \sigma_i(\varepsilon) v_e(\varepsilon) n_e(\varepsilon) d\varepsilon}{\int_0^\infty n_e(\varepsilon) d\varepsilon}, \qquad (3)$$

where $n_e(\varepsilon)d\varepsilon = \frac{2N_e}{\sqrt{\pi}}(\frac{\varepsilon}{\varepsilon_m})^{1/2} e^{-\varepsilon/\varepsilon_m} d(\frac{\varepsilon}{\varepsilon_m})$ for the assumed Maxwellian distribution. Replacing the upper integral in Equ. 3 by a summation and utilizing the measured relative cross section from Ref. 11 calibrated with the absolute value at 38 eV from Ref. 12, the dependence of rate coefficient on electron temperature was obtained from Equ. 4.

$$k_i \cong \frac{2}{\varepsilon_m \sqrt{\pi m_e}} \sum_0^{50eV} \sigma_i(\varepsilon) \varepsilon^{1/2} e^{-\varepsilon/\varepsilon_m} \Delta\varepsilon \ , \qquad (4)$$

The corresponding curve for Xe^+/Xe was obtained by an analogous process, using the cross section data of Ref. 13. For $n_{60} = 10^{12}$ cm^{-3}, $\varepsilon_p = 30$ eV, $N_e = 4\times10^{11}$ cm^{-3}, and $N_p/N_e = 0.15$, the production rate of C_{60}^+ in the high magnetic field region by electron impact is estimated to be $\sim1\times10^{17}$ cm^{-3}s^{-1}. A similar calculation for xenon atoms at the same density of 10^{12} cm^{-3} yields a Xe^+ production rate one order of magnitude lower.

Recombination

For an efficient rare gas ion engine, ion current densities at the thruster walls as little as 7% of the beam current density at the extraction grid plane have been demonstrated.[14] Ion-electron recombination in the plasma by the process $R^+ + e \rightarrow R + h\nu$ is slow due to the small cross section of $\sim10^{-21}$ cm^2.[15] Even at the low densities in rare gas ion engines, dissociative recombination via $R_2^+ + e \rightarrow R + R^*$ will be the dominant recombination process. The limiting step is $R^+ + R + R \rightarrow R_2^+ + R^*$. Xenon has a measured rate constant for the latter reaction of 3.6×10^{-31} cm^{6}s^{-1} at 300 K,[15] leading to an estimated Xe_2^+ production rate in a typical xenon ion engine of 1×10^5 cm^{-3}s^{-1}. Recombination is clearly insignificant as a Xe^+ loss mechanism in these engines, since Xe^+ extraction rates over a 10-30 cm diameter grid set are normally in the range 2×10^{18}- 2×10^{19} s^{-1}.

In a fullerene engine, electron recombination must be included in the analysis. Although a measured cross section for electron recombination with C_{60}^+

$$C_{60}^{+} + e \rightarrow C_{60} \qquad (5)$$

is not presently available, comparison with other systems suggests a value of 10^{-13} - 10^{-12} cm^2 at thermal energies. The rate coefficient for molecular ions normally decreases as $\varepsilon^{-1/2}$ up to energies of ~0.2 eV and as $\varepsilon^{-3/2}$ thereafter.[15] Because of the ability of C_{60} to accommodate the recombination energy without dissociating, its rate coefficient may not depend as strongly on electron energy. For migration of nascent C_{60}^{+} ions to the extraction grids over a distance of 5 cm at the Bohm velocity, the transit time is ~70 μs, or ~14 μs for a distance of 1 cm. During this transit the primary electron density and magnetic field strength decrease while the Maxwellian electron temperature and primary electron energy remain approximately constant. The primary electron density is roughly 10× lower than the plasma density. For an electron temperature of 3 eV, the electron recombination probability for C_{60}^{+} during transit, $k_r N_e t_d$, will be on the order of unity, a serious problem since the electron impact ionization rate may be an order of magnitude lower near the grids than near the hollow cathode.[17]

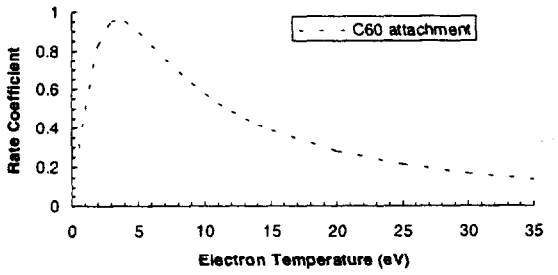

Figure 1. Electron attachment rate coefficient for C_{60}.

Ion-ion "recombination", a non issue for xenon thrusters,

$$C_{60}^{+} + C_{60}^{-} \rightarrow 2C_{60} \qquad (6)$$

must also be considered. The cross section and rate constant for Equ. 6 can be estimated from[17]

$$\sigma(E_0) = \pi R \left(1 - \frac{z_1 z_2 e^2}{R E_0}\right) \qquad (7)$$

and

$$k_r = \bar{g} R^2 \left(1 + \frac{|z_1 z_2| e^2}{R k T_i}\right) \qquad (8)$$

where $\bar{g} = \left(\frac{8\pi k T_i}{\mu}\right)^{1/2}$.

The result is $k_{+/-} \sim 2\times10^{-9}$ cm^{3}s^{-1}, only slightly larger than the hard sphere cross section because the ion temperature is much higher than thermal. Comparison with rate coefficients for C_{60} electron attachment, ionization to C_{60}^{+} and electron recombination with C_{60}^{+} indicates that C_{60}^{+} - C_{60}^{-} recombination is slow compared to these processes, because electrons have much higher velocity than fullerene ions. This is also true of the reaction

$$Xe^{+} + C_{60}^{-} \rightarrow C_{60} + Xe\,. \qquad (9)$$

Unfortunately, the cross section is not presently available for several other potentially important processes, such as electron collision with C_{60}^{-} to produce C_{60}^{+} or C_{60}.

Electron Attachment

A serious difficulty for the C_{60}^{+} ion engine concerns the rate and unusual properties of C_{60} electron attachment. The cross section for electron attachment is large over the range 0-13 eV, exceeding that of electron impact ionization even at 13 eV. It averages 9×10^{-15} cm^2 over the electron energy range 0-7 eV. The relative rate coefficient for electron attachment as computed from an expression analogous to Equ. 4, using cross section data from Ref. 17, is given in Fig. 1. The electron attachment process has a very high rate. For a Maxwellian distribution with an electron temperature of 3 eV, the rate of

$$C_{60} + e \rightarrow C_{60}^{-} \qquad (10)$$

is 2×10^{17} cm^{-3}s^{-1} if $n_{60} = 1\times10^{12}$ cm^{-3} and $N_m = 2\times10^{11}$ cm^{-3}. Essentially complete conversion of C_{60} to C_{60}^{-} can occur within a residence time of just 10 μs in such a region if N_m dominates over N_p.

Charge Transfer

If xenon is present in the main discharge and C_{60} is injected into the engine, the rate of charge transfer from rare gas ions like Xe^{+} to C_{60} must be considered. Indeed, charge transfer from rare gas atoms to C_{60} or another heavy molecule could conceivably be used for the production of massive, extractable ions with potentially high engine thrust and efficiency. A

charge transfer engine could be similar to a typical ion engine in using rare gas hollow cathodes and magnetic confinement of high energy electrons in a rare gas discharge. Charge transfer will leave less internal energy in the ionized species than electron impact ionization.

C_{60} has a large charge transfer cross section in collisions with rare gas ions, and no fragmentation has been observed at collision energies below 20 eV, even after several milliseconds. The Langevin rate constant, k_{ct}, for the transfer of charge from Xe^+ to C_{60}

$$Xe^+ + C_{60} \rightarrow Xe + C_{60}^+ \qquad (11)$$

depends on the polarizability of C_{60}, α, and the reduced mass, μ.

$$k_{ct} = 2\pi e\left(\frac{\alpha}{\mu}\right)^{\frac{1}{2}}. \qquad (12)$$

For the polarizability of $4/3\times10^{-24}$ cm^3,[18] the result is $k_{ct}=2.0\times10^{-9}$ cm^3s^{-1}, an unusually large reaction rate constant for charge transfer. The product kN_{Xe^+} gives $1/t_d$ where t_d is the average time required for conversion of individual C_{60} molecules in the drift region to C_{60}^+ via the charge exchange reaction with Xe^+. N_{Xe^+} is the Xe^+ density, or plasma density, which is on the order of 4×10^{11} cm^{-3} near the screen grid in a conventional ion engine discharge chamber. The plasma density could be tailored via the discharge current to provide an adequate supply of Xe^+ to the drift region, and an appropriate supply of Xe^+ and C_{60}^+ to the extraction grids. As a result, the optimum plasma density at the entrance to the drift region could be substantially higher than 4×10^{11} cm^{-3}.

A C_{60} molecule is likely to undergo charge transfer if it remains in the drift region for ≥1.3 ms. The average velocity of C_{60} at 800K, approximately the temperature necessary to produce an appropriate sublimation rate, is 1.5×10^4 cm/s. For a 25 cm diameter thruster, the transit time across the drift region (perpendicular to the ion flow direction) is 1.6 ms, enough time to allow conversion to C_{60}^+ with good probability. For the same plasma density, a larger diameter thruster provides greater margin to ensure that neutral C_{60} molecules do not transit the drift region unreacted, to deposit on the wall surface. C_{60} deposits will form due to (a) molecules which travel across the drift section diameter without undergoing ionization, (b) ion-electron recombination which occurs before ion extraction, and (c) anode impingement of C_{60}^- formed by electron attachment. Active heating of the thermally isolated wall of the drift section would help to control this problem. Fragmentation is highly improbable during transit, due to the low electron temperature. The ratio of C_{60} ions to xenon ions could be varied, within limits, by adjusting the solid C_{60} temperature to change its sublimation rate, if charge transfer is the dominant source of C_{60}^+.

A comparison of charge transfer, electron attachment, and recombination reaction rates indicates immediately that charge transfer is slow compared to the reactions involving electrons, due to the high electron mobility. It cannot be ignored in the chemical analysis of a thruster containing both Xe and C_{60}, however, and Equ. 4 will be included in the subsequent analysis.

Positive Fullerene Ion Propulsion

The construction of a viable ion engine utilizing C_{60}^+ must involve the direct injection of C_{60} into a region containing energetic electrons such that ionization dominates electron attachment. A ring of injectors containing solid C_{60} would direct the sublimated C_{60} molecules into the appropriate region. None of the previous engine designs has done this. The density of C_{60} can be estimated from

$$N_{60} = \frac{4S}{\pi dsv}, \qquad (13)$$

For a 25 mm long region in a 10 cm engine, a sublimation rate of 5×10^{17} $cm^{-2}s^{-1}$ gives an average C_{60} density in the drift region of 1.7×10^{12} cm^{-3}. Once formed in the region with high primary electron density, C_{60}^+ must be extracted before electron recombination occurs. The high rate coefficient for C_{60} ionization by primary electrons (about 10× higher than for Xe ionization) aids in this respect, since the discharge chamber volume and its length to diameter ratio can be relatively small, reducing ion losses to the wall and average distance between formation and extraction sites. As discussed above, the electron recombination cross section has not been measured, but the rate coefficient is expected to decrease as $\varepsilon^{-3/2}$ over most of the electron energy distribution function, with a value of about 10^{-6} cm^3 s^{-1} at thermal energies. If k_r decreases as $\varepsilon^{-1/2}$ up to 0.25 eV and $\varepsilon^{-3/2}$ thereafter, an estimate of the product $k_r n_e(\varepsilon)\Delta\varepsilon\Delta t$ yields $\sim4\times10^{-8}N_e\Delta t_d$ for the probability of recombination during transit to the extraction region. For N_e =

3×10^{11} cm^{-3}, ε_m = 3 eV, N_i/N_m = 1.1, and transit at the Bohm velocity, given by[7]

$$v_b = \sqrt{\frac{\varepsilon_m N_i}{em_i N_m}}, \qquad (14)$$

the probability that C_{60}^+ will undergo electron recombination is ~0.2d, for d in centimeters.

A schematic diagram for an ion engine expelling positive fullerene ions is given in Fig. 2. The cathode tip has been moved forward toward the screen grid and the magnetic field is highly divergent compared to typical ion engines (see, for example, designs in Refs. 2,10,14) to reduce the ionization volume and position the ionizing region closer to the extraction grids. The ion density, primary and Maxwellian electron density, and plasma potential are decreasing functions from cathode tip to screen grid, whereas Maxwellian electron temperature and primary electron energy are relatively constant.[7] With a typical distance from production site to extraction site of about 1 cm, the probability of recombination is small. The baffle disc shown in the diagram might protect the screen grid from erosion by helping to establish proper trajectories of cathode ions and electrons, but may not be necessary. C_{60}^-, which will inevitably be formed in significant numbers, will not strike the screen grid or be extracted due to repulsion by the screen grid sheath. The anions will be collected by anode surfaces, with deposit growth somewhat limited by electron and ion sputtering at the anode surface.

Due to the large cross section for charge exchange in the plume involving C_{60} and C_{60}^+, the production and migration of charge exchange ions to the spacecraft may be a more serious problem than in the case of xenon thrusters.

Negative Fullerene Ion Propulsion

The very high rate of electron attachment to C_{60} in the low-field region suggests the potential utility of a C_{60}^- ion engine. As in the C_{60}^+ case, the C_{60} would be injected. Even with the small discharge volume of the design indicated by Fig. 2, when C_{60} is injected a substantial fraction of available fullerene ionic species will be C_{60}^-. In a conventional ion engine, the extraction of positive ions leaves a negative space charge which is readily moderated by the rapid migration of electrons toward regions with more positive potential. The extraction of negative ions will increase the ratio of positive to negative charge, attracting additional electrons to the region.

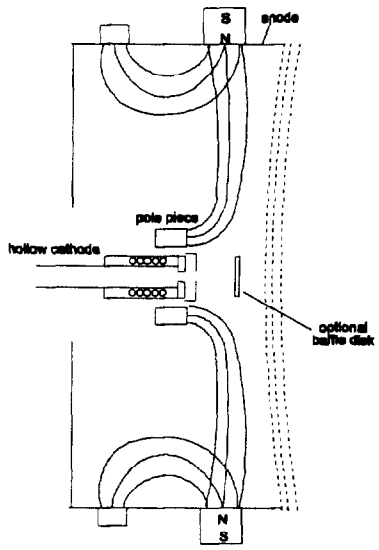

Figure 2. Schematic diagram of gridded ion engine which reduces residence time. C_{60} sublimator and full magnetic field circuit not shown.

To achieve a quasi-neutral plasma near the extraction grids of a negative ion engine, positive ions (primarily R^+ and C_{60}^+) must be provided by the discharge in numbers sufficient to balance the combination of C_{60}^- and free electrons. Since electron mobility is far higher, the near-grid region should acquire a relatively negative potential to encourage positive ion migration and limit electron density, thereby maintaining quasi-neutrality. To limit electron extraction through the grid system, a magnetic field ≥10 Gauss is required with field lines parallel to the grids such that electrons must cross the field lines to be extracted. The electron cyclotron radius is given by

$$r_c(cm) = 3.37\sqrt{\frac{\varepsilon_m(eV)}{B(gauss)}}. \qquad (15)$$

For 3 eV electrons and a magnetic field of 15 gauss, r_c = 1.5 cm. The presence of C_{60} near the grids will result in a lower electron temperature there compared to conventional ion engines. Like the C_{60}^+ version of Fig. 2, a C_{60}^- ion engine could have hollow cathode and main discharge based on a rare gas (krypton, xenon, or even argon), with C_{60} injected into the plasma. The plasma can be divided into at least three principal zones, (*i*) hollow cathode region, (*ii*) injection region, and (*iii*) the plume, in which neutralization by positive ions must occur.

Plume neutralization may be accomplished by injecting positive ions created in a simplified ion

engine. Although the ion current density available from a plasma

$$r_c\,(cm) = 0.344 N_e e\sqrt{2kT_e/m_i}\ , \qquad (16)$$

(N_e refers to the plasma center) is more than adequate, Child's law sets a limit to the extracted current which is proportional to $AV^{3/2}/\sqrt{m_i}$. Equating the absolute value of extracted current from main discharge chamber and neutralizer operating on C_{60} and Kr, respectively, leads to the result $V_N = 0.48 V_{60}(A_M/A_N)^{2/3}$. If the emitting areas are equal the neutralizer extraction voltage must be about half of the C_{60} extraction voltage and the neutralizer will consume about one quarter of the expended extraction energy. Neutralizer energy consumption is reduced as its emitting area increases, but the required geometry and energy consumption is a very significant disadvantage for the negative ion engine since high thrust density and high efficiency are central goals for spacecraft propulsion. This type of design is a potentially useful source of intense beams of C_{60}^- and other negative ions derived from parent molecules with large electron attachment cross sections, for terrestrial applications.

Table 1. Computed rate coefficients.

reaction	rate coefficient (cm^3s^{-1})
Equ. 2	1.05×10^{-6};1.56×10^{-9}
Equ. 5	0.0;1.0×10^{-7}
Equ. 6	3.95×10^{-9}
Equ. 9	5.04×10^{-9}
Equ. 10	0.0;1.41×10^{-7}
Equ. 11	8.10×10^{-9}
$Xe + e \rightarrow Xe^+ + 2e$	1.00×10^{-7};0.0

CHEMKIN Analysis

A standard program for chemical kinetics analysis, CHEMKIN, was adapted for a preliminary analysis of the chemistry of the fullerene ion engine of Fig. 2. The rate constants used for the analysis are listed in Table 1. Where two rate coefficients are given, these pertain to primary electrons (ε_p = 30 eV) and Maxwellian electrons (ε_m = 4 eV), respectively.

The parameters for Xe, Xe^+, primary and Maxwellian electrons in region (*i*) were assumed, with the values indicated in Table 2. These parameter values are in the normal range expected for a conventional xenon ion engine. The simulation injected C_{60} into region (*ii*) as the hollow cathode region (*i*) species flow into it. Positive ions were given a 10 μs residence time, with replenishment of the parent neutral occuring at the extraction rate × 1.2, corresponding to a utilization of 83% for Xe^+ and C_{60}^+ species. Electron impact ionization produced C_{60}^+ and Xe^+ in region (*ii*), with Maxwellian electron attachment to C_{60} producing the C_{60}^- in the region. It was assumed that each ionizing collision between a 30 eV primary electron and an atom or molecule would transform the primary into a Maxwellian with ε_m = 4 eV. Replenishment of primary electrons in region (*ii*) occured with N_p constant in region (*i*) at the value in Table 2, allowing primary electrons to transfer only in the direction $i \rightarrow ii$, with a 0.4 μs residence time in

Table 2. Input parameters for CHEMKIN calculation.

parameter	input value
N_{Xe}	1.8×10^{12} cm^{-3}
N_{60}	1.8×10^{12} cm^{-3}
N_m	2.0×10^{11} cm^{-3}
ε_m	4 eV
N_p	4×10^{10} cm^{-3}
ε_p	30 eV
n_{60}^+	0
n_{60}^-	0
N_{Xe^+}	2.4×10^{10} cm^{-3}

region (*i*). For the results shown in Fig. 3, the plasma was constrained to be quasi-neutral, i.e. Maxwellian electron density was adjusted to keep the sum of total charge near unity. These electrons can readily adjust their concentration, under the influence of small potential gradients, to maintain quasi-neutrality. Without this condition, the sum of total charge would quickly become negative as positive ions are extracted and Maxwellian electrons accumulate, many attaching to C_{60} to form C_{60}^-. Figure 3 indicates that C_{60}^+ and C_{60}^- build up quickly during the first 10 μs of the simulation, with C_{60}^+ the most abundant ion, easily surpassing Xe^+ and C_{60}^-. This occurs despite the very high C_{60} attachment rate because quasi-neutrality maintenance dictates a rapid Maxwellian electron loss rate which raises the primary to Maxwellian electron ratio, favoring ionization over attachment. The results of Fig. 3 are preliminary, and this is especially the case given that the results indicate difficulty in meeting the quasi-neutrality contraint and achieving steady state conditions.

Concluding Remarks

The failure to demonstrate a working laboratory C_{60} engine during the past 5 years has suggested that a fullerene ion engine with better performance than the current xenon standard cannot be produced. Analysis of the kinetics of charged fullerene formation and destruction in the discharge chamber reveals why

previous designs have not worked. New designs have been proposed which will help to alleviate the problems. It is believed that the new approach will lead to C_{60} engines with far better performance figures.

Results of this preliminary CHEMKIN analysis suggest that C_{60}^{+} can be produced and extracted efficiently in a fullerene engine, provided that the engine geometry, C_{60} injector design, and magnetic

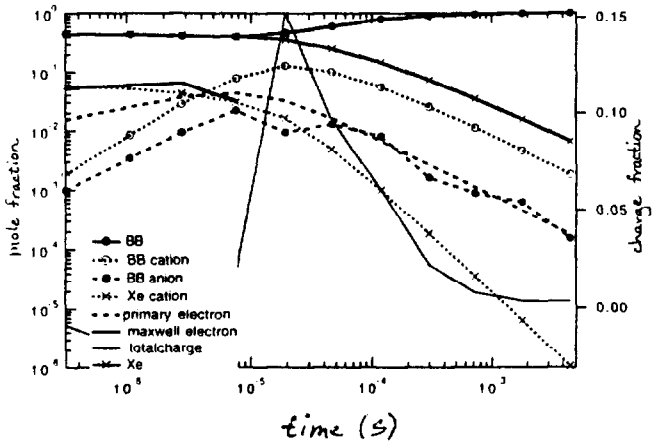

Figure 3. Output of CHEMKIN calculation for charge constrained case (see text).

field are tailored for this purpose. C_{60}^{-} could be produced efficiently for extraction because of the very high electron attachment rate coefficient. However, neutralization of the negative ion beam is costly in terms of the energy and volume required.

The fullerene ion engine represents an enabling technology that could dramatically increase ion engine thrust density and thrust per unit of input power in the desired range of specific impulse. It has the potential to substantially reduce travel times for electric orbit transfer, interplanetary missions, and satellite repositioning.

References

1. Leifer, S.D., Rapp, D., and Saunders, W.A., "Electrostatic Propulsion Using C_{60} Molecules," *J. Propulsion and Power*, Vol. 8, No. 6, 1992, pp. 1297-1300.

2. Beattie, J.R., Matossian, J.N., and Robson, R.R., "Status of Xenon Ion Propulsion Technology," *J. Propulsion and Power*, Vol. 6, No. 2, 1990, pp. 145-150.

3. M.W. Crofton, "Evaluation of the United Kingdom Ion Thruster," *J. Spacecraft and Rockets*, Vol. 33, No. 5, 1996, pp. 739-747.

4. Anderson, J.R., Fitzgerald, D., Leifer, S., and Mueller, J., "Design and Testing of a Fullerene RF Ion Engine," AIAA Paper 95-2664, July 1995.

5. Nakayama, Y. and Takegahara, H., "Fundamental Experiments of C_{60} Application to Ion Thruster," IEPC Paper 95-88, Sept. 1995.

6. Anderson, J.R. and Fitzgerald, D., "Fullerene Propellant Research for Electric Propulsion," AIAA Paper 96-3211, July 1996.

7. Masek, T.D., "Plasma Properties and Performance of Mercury Ion Thrusters," *AIAA J.*, Vol. 9, No. 2, 1971, pp. 205-212.

8. Foltin, M., Lezius, M., Scheier, P., and Märk, T.D., "On the Unimolecular Fragmentation of Fullerene Ions: The Comparison of Measured and Calculated Breakdown Patterns," *J. Chemical Physics*, Vol. 98, No. 12, 1993, pp. 9624-9634.

9. Sundar, C., Bharathi, A., Harihan, Y., Janaki, J., Sankare Sastry V., and Radhakrishnan, T., "Thermal Decomposition of C_{60}," Solid State Communications, Vol 84, No. 8, 1992, p. 823, and references therein.

10. Kaufman, H.R., "Technology of Electron-Bombardment Ion Thrusters," *Advances in Electronics and Electron Physics*, Marton, L., ed., Vol. 36, Academic, New York, 1974, 390 pp.

11. Matt, S., Dünser, B., Lezius, M., Deutsch, H., Becker, K., Stamatovic, A., Scheier, P., and Märk, T.D., "Absolute Partial and Total Cross-section Functions for the Electron Impact Ionization of C_{60} and C_{70}," *J. Chem. Phys.*, Vol. 105, No. 5, 1996, pp. 1880-1896.

12. Baba, M.S., Narasimhan, T.S.L., Balasubramanian, R., and Mathews, C.K., "Appearance Potential and Electron Impact Ionisation Cross-section of C_{60}, *Int. J. Mass Spectrom. Ion Processes*, Vol. 114, 1992, pp. R1-R8.

13. Rapp, D. and Englander-Golden, P., "Total Cross Sections for Ionization and Attachment in Gases by Electron Impact. I. Positive Ionization," *J. Chemical Physics*, Vol. 34, No. 5, 1965, pp. 1464-1479.

14. Sovey, J.S., "Improved Ion Containment Using a Ring-Cusp Ion Thruster," *J. Spacecraft and Rockets*, Vol. 21, No. 5, 1984, pp. 488-495.

15. Raizer, Y.P., *Gas Discharge Physics*, Springer-Verlag, Berlin, 1991.

16. Jaffke, T., Illenberger, E., Lezius, M., Matejcik, S., Smith, D., and Märk, T.D., "Formation of C_{60}^{-} and C_{70}^{-} by Free Electron Capture. Activation Energy and Effect of the Internal Energy on Lifetime," *Chem. Phys. Lett.*, Vol. 226, 1994, pp. 213-218.

17. Weston, R.E. Jr., and Schwarz, H.A., *Chemical Kinetics*, Prentice-Hall, Englewood Cliffs, N.J., 1972, see pp. 63-4, 88-9.

18. Kaplan, T., Rasolt, M., Karimi, M., and Mostoller, M., "Numerical Simulation of He^{+} and Li^{+} Collisions with C_{60}," *J. Phys. Chem.* Vol. 97, No. 23, 1993, pp. 6124-6126.